Technical Report on the NASA Research Grant NAG5-13388 "**Validation of mean absolute sea level of the North Atlantic obtained from drifter, altimetry and wind data**" conducted at the IPRC/SOEST, University of Hawaii, 05/01/03-09/30/03

1. Introduction to the method

Mean absolute sea level reflects the deviation of the ocean surface from geoid due to the ocean currents and is an important characteristic of the dynamical state of the ocean. Values of its spatial variations (order of 1 m) are generally much smaller than deviations of the geoid shape from ellipsoid (order of 100 m) that makes the derivation of the absolute mean sea level a difficult task for gravity and satellite altimetry observations.

Technique used by Niiler et al. (2003a) for computation of the absolute mean sea level in the Kuroshio Extension was then developed into more general method and applied by Niiler et al. (2003b) to the global ocean (Fig.1). The method is based on the consideration of balance of horizontal momentum in its simplest form:

$$d\mathbf{V}/dt + \mathbf{f} \times \mathbf{V} = - g \nabla h + \partial\tau / \partial z /\rho_0 + \text{H.O.T.}, \qquad (1)$$

where f is the Coriolis parameter and g is a gravitational constant. After neglecting the higher order terms (H.O.T.), horizontal gradient of the mean sea level can be estimated as

$$\nabla\langle h\rangle = \underbrace{-(d\mathbf{V}/dt + \mathbf{f} \times \mathbf{V})/g}_{\text{I}\quad\text{II}} \underbrace{- \nabla h'}_{\text{III}} + \underbrace{\partial\tau / \partial z /(\rho_0 g)}_{\text{IV}} \qquad (2)$$

Acceleration (I) and Coriolis (II) terms are estimated using velocities derived from Lagrangian drifter data received from the NOAA/AOML, where they were acquired, quality controlled and interpolated onto 6-hourly intervals. Subtraction of the anomalous sea level gradient (III) corrects the bias in the drifter ensemble due to its nonuniform temporal distribution and interannual variations of surface circulation. Term (IV) describing vertical divergence of the

Ekman stress was estimated using NCAR/NCEP reanalysis wind data at 10 m level and parameterization formula suggested by Ralph and Niiler (1999; thereafter RN99). Originally derived for Ekman velocities, it can be rewritten for (IV) in the complex notation as

$$\partial\boldsymbol{\tau} / \partial z = C \cdot f^{1/2} \cdot \mathbf{W} \cdot \exp\{\mathbf{i}\varphi_o\}, \qquad (3)$$

where $\mathbf{W}$ is the wind vector and the angle $\varphi_o = 36^0 \cdot \mathrm{sign}(\theta)$ is constant for each of the two hemispheres.

Among advantages of the method are clear definition of the "mean" as a time average over specific time periods and high, mesoscale, spatial resolution. Such resolution helps to reveal the complexity of the mean surface circulation in many regions. Example of the North Atlantic is shown in Figure 2.

Largest errors in (1) are expected in the term IV. These errors are both due to the uncertainties in the wind data and parameterization formula. Additional errors occur in the sea level anomaly (III) field, generally, oversmoothed by the Aviso mapping procedure.

This document reports the results of the study of these three sources of uncertainties. For the convenience of the study the geographic area was expanded to include all regions covered with the data. Using recently released preliminary data of the GRACE project, we were able to improve the Ekman parameterization suggested by Ralf and Niiler (1999). Improvement is particularly significant at high latitudes. By comparing between the Ekman parameterizations obtained for the NCAR/NCEP reanalysis winds and for the QuikSCAT satellite winds, we show that results are sensitive to the product and suggest future multi-variable analysis. Section 4 describes biases that may occur in the data statistics when too simple methods are used to eliminate the difference in spatiotemporal spectra of drifter, satellite altimetry and wind data caused by different resolutions of the three datasets.

2. Ekman parameterization

Among many sources of the potential errors in the mean sea level computed by integrating (2), the most important one is expected to be related to the way how Ekman currents (or stress) are parameterized. RN99 derived their formula (3) for low latitude regions of relatively low eddy activity and steady winds in the North and South Pacific. Their formula gives optimal latitude-dependent angle and coefficient between the mean NCAR/NCEP wind and Ekman currents, the latter being estimated using mean drifter velocities and climatological mean geostrophic velocities referenced to 1000 m depth. Figure 3 shows that in terms of horizontal curl of vertical divergence of the Ekman stress the formula gives consistent estimates in all ocean basins at least between 40^0S and 40^0N.

However, it is not clear if:

- the same formula can be applied to the high latitudes;
- coefficients are not very sensitive to the frequency of the signal;
- relation between the wind and Ekman velocity/stress is linear at all.

Questions on the accuracy of (3) also remain because of vague definitions of the mean ("drifter-ensemble-mean" and "Levitus-climatology-mean") used by RN99. Being weaker than typical ocean currents, Ekman currents, however, can give rise to large errors in the sea level when integrated over large distances.

Recently, first results from the GRACE satellite mission provided improved model of the Earth's gravity field (http://www.csr.utexas.edu/grace/). This geoid model was then used to compute the mean absolute sea level from accumulated during the last decade satellite altimetry. The products developed in various institutions are summarized and intercompared at http://iprc.soest.hawaii.edu/~nikolai/Globe/GRACE/GRACE.html. For this study we used products from the NASA Goddard Space Flight Center (courtesy of Brian Beckley, Figure 4) and Jet Propulsion Laboratory (courtesy of Victor Zlotnicky, Figure 5). Figures 4 and 5 illustrate the fact that effective spatial resolution of the GRACE data is limited to 400-500 km. However, larger scales seem to be trustworthy. Figure 6 shows that biggest difference between the GRACE (Fig.5) and NMM03 (Fig.1) mean sea levels is in the Southern ocean and reaches 130 cm across

the Antarctic Circumpolar Current (ACC). It was also found that zonal gradients of the mean sea level estimated from (2) with RN99 do not vanish while integrated along quasi-zonally contour around Antarctida. Unbalanced sea level gradient along the ACC also results in average differences between the oceans seen in Figure 6. Other differences can be attributed to different scales of spatial resolution (most obvious around the Gulf Stream, Kuroshio and Agulhas jets) and effects of coastal friction and upwelling.

As a first step we use (2) to estimate $\mathbf{T} = \partial\tau / \partial z /(\rho_0)$ at drifter locations and times. Term $\nabla\langle h\rangle$ is estimated from the GRACE-based mean sea level (Fig.5), terms (I) and (II) come from drifters and term (III) is from the Aviso/Enact grided sea level anomaly data. Technically, the procedure was designed to eliminate high-level noise in the data without oversmoothing the results. It is easy to show that coefficients of a simple rotate-and-rescale transform

$$T_x = a\cdot W_x - b\cdot W_y,$$
$$T_y = b\cdot W_x + a\cdot W_y, \qquad (4)$$

minimize $\langle\langle\langle(\mathbf{T}- A\cdot\mathbf{W})^2\rangle\rangle\rangle$ ($\mathbf{W}$ is the wind vector) when

$$a=\langle\langle\langle\mathbf{T}\cdot\mathbf{W}\rangle\rangle\rangle/\langle\langle\langle\mathbf{W}\cdot\mathbf{W}\rangle\rangle\rangle,$$
$$b=\langle\langle\langle\mathbf{k}\times(\mathbf{T}\times\mathbf{W})\rangle\rangle\rangle/\langle\langle\langle\mathbf{W}\cdot\mathbf{W}\rangle\rangle\rangle, \qquad (5)$$

where k is an upward looking unity vector. Then optimal angle and coefficient between vectors $\mathbf{T}$ and $\mathbf{W}$ are:

$$\tan(\text{angle}) = b/a,$$
$$\text{coefficient} = \text{sqrt}(a^2+b^2). \qquad (6)$$

Thus defined coefficients take into account both correspondence between mean vectors and their covariance.

Averaging $\langle\ldots\rangle$ has been done in a number of subsequent steps. First, all instantaneous data were sorted according to local latitude and instantaneous wind speed and averaged ($\langle\ldots\rangle$) within the bins 1^0 latitude x 1 m/s. Second, values of $\langle\mathbf{T}\cdot\mathbf{W}\rangle$, $\langle\mathbf{k}\times(\mathbf{T}\times\mathbf{W})\rangle$, $\langle\mathbf{W}\cdot\mathbf{W}\rangle$, $\langle\mathbf{T'}\cdot\mathbf{W'}\rangle$, $\langle\mathbf{W'}\cdot\mathbf{W'}\rangle$ and $\langle\mathbf{T'}\cdot\mathbf{T'}\rangle$, were additionally smoothed with the running 9^0 latitude x 3 m/s mean ($\langle\langle\ldots\rangle\rangle$) and correlation coefficient was calculated as $CC=\langle\langle\mathbf{T'}\cdot\mathbf{W'}\rangle\rangle/(\langle\langle\mathbf{W'}\cdot\mathbf{W'}\rangle\rangle \cdot \langle\langle\mathbf{T'}\cdot\mathbf{T'}\rangle\rangle)^{1/2}$. Finally, at each latitude $\langle\langle\mathbf{T}\cdot\mathbf{W}\rangle\rangle$, $\langle\langle\mathbf{k}\times(\mathbf{T}\times\mathbf{W})\rangle\rangle$ and $\langle\langle\mathbf{W}\cdot\mathbf{W}\rangle\rangle$ were

averaged over the bins containing more than 100 drifter fixes (that defined extreme latitude limits) and having CC > 0.1. These values were than substituted into (5) and (6) and optimal angle and coefficient of **T** to **W** are shown in Figure 7.

It is seen that qualitative correspondence with RN99 is fairly good. For some unclear reasons correspondence in the angle is especially good at 20-50^{0}N and correspondence in the coefficient is especially good at 10-50^{0}S. Qualitative correspondence with RN99 seems to be even better in terms of Ekman velocities (Fig. 8). Indeed, jump in the angle across the equator looks more significant than its variations away from the equator. Coefficient differs from RN99 by less than 30% between 60^{0}S and 70^{0}N (except for the narrow equatorial belt where the use of geostrophy is tricky). However, after more careful look, in both hemispheres Ekman velocities are almost perpendicular to the wind at low latitudes but become more in the direction of the wind around 60^0 latitude. Such a monotonic behavior of the angle can be explained by the increase of the Ekman layer thickness with the growing latitude. The thicker the Ekman layer the closer the Ekman currents measured by drifters at 15 m depth to their values at the sea surface. Interestingly, the 30^0 angle suggested at 60^0 latitudes cannot be explained by the Ekman layer model with any constant mixing coefficient, but it does can exist in the model where mixing coefficient grows with the depth. Light blue lines in Figures 7 and 8 are drawn by reversing the latitude axis. In terms of the angle correspondence between the two hemispheres is very good (two blue lines deviate not more than few degrees from each other). One can see that even in terms of **T** (Fig.7) the angle changes sharply by about 30^0 across the equator. We assume that equatorial dynamics can involve higher order terms neglected here. Simple rule is that **the angle between T and wind is approximately equal to the value of local latitude**.

The following tendencies are seen in the coefficients in Figs. 7 and 8. New coefficients are smaller than suggested by RN99 at 30^{0}S and 30^{0}N, latitudes of the weakest winds. New coefficients are larger than suggested by RN99 at the equator where winds are strong and steady and at 60^{0}S and 60^{0}N, where atmospheric eddies are very active, especially, the winter storms. One explanation can be that actual relation is nonlinear to the wind speed. Among various possible sources of non-linearity most credible are the actual relation between the wind vector and the wind stress and influence of the wind strength on the intensity of mixing in the upper

ocean. When the former fact is well known from the bulk formula the latter one is illustrated by Figure 9, which shows that in the northern/southern hemisphere **T** (and also $\mathbf{V}_E$) at 15 m rotates counterclockwise/clockwise as wind becomes higher. Such a behavior is consistent with the suggestion that higher wind enhances the mixing, which increases the effective Ekman scale and changes values of the Ekman spiral at 15 m toward those at the sea surface. This process can also be responsible for the larger coefficients (lower panel in Fig.9) at higher winds. More details on the dependence of T on the wind strength are shown in Figure 10 and discussed at http://iprc.soest.hawaii.edu/~nikolai/Globe/GRACE/OptEkman-GRACE.html.

Remarkable in the meridional distribution of coefficients are maxima at 65^0S and 55^0N. More extensive study is required to understand what makes these high latitudes so special and why the peak in the south is much more pronounced than in the north. Possible mechanisms can be related to the air-sea heat fluxes contributing to the mixing and also the effect of the Stokes' drift in the wind waves field (McWilliams and Restrepo, 1999).

3. Sensitivity of Ekman parameterization to the wind product: QuikSCAT vs NCEP

Procedure similar to the one described in the previous section was applied to the data of QuikSCAT satellite wind data. The data (Level 2 sea wind vectors) are on spatial 25 km grid and were downloaded by Dr. Jan Hafner (IPRC/SOEST, University of Hawaii) from the public site of NASA JPL PO DAAC and interpolated (linearly) onto exact locations and times of drifters. Optimal coefficient and angle of vector T to the QuikSCAT wind vector are shown in Figure 11, which reveals significant differences in both parameters from Figure 9. Taking into account that the QuikSCAT dataset starts in 1999, temporal distribution of the data is quite different from the one described in Section 2 that can partially be the source of discrepancies between the two statistics. The other reason for the difference can be the difference between the two wind products. To eliminate the effect of temporal bias, we compared QuikSCAT winds with the contemporaneous NCAR/NCEP wind vectors and results are shown in Figure 12. Correlation coefficient (Fig.12a) mainly varies between 0.2 and 0.8 and higher for higher wind speeds, probably defined by the relative level of noise. R.m.s. deviation (Fig.12b) between the two winds

is in the range from 2 to 8 m/s and exceeds the formal errors of the QuikSCAT winds, which are announced to be 2 m/s in the wind speed and 20^0 in the wind direction. Ratio of the r.m.s. deviation to the wind speed in the selected latitude-wind-speed bin is shown is Fig.12c and 0.5 is its rather typical value. Angle (Fig.12d) between the wind vectors is typically $\pm$ 2-5^0, but at some latitudes and wind speeds exceeds $\pm$ 10^0. Coefficient between the winds (Fig.12e) is generally larger than 0.6 and less than 1 (QuikSCAT winds are stronger). Although Figures 12d and 12e indicate differences between the wind scale and direction comparable to the formal errors of the QuikSCAT dataset, they in fact reveal remarkable systematic differences between the two wind products. Further comprehensive study is required to understand how these systematic differences are distributed along the spatiotemporal spectra, what fraction of the error is due to the differences in physical models used to describe the atmospheric boundary layer and whether these errors can be reduced.

4. Biases in the statistics based on combined datasets having different spatiotemporal resolution

Accuracy of the momentum balance described in Section 1 is affected by the differences between spectral properties of three absolutely independent datasets (drifters, satellite altimetry and winds) used jointly. Correction of the imbalance with underthought method produces a danger of biases, some of which will be considered in this Section.

Drifters are proved to provide measurements of the surface velocity at good accuracy. However, their Lagrangian data are distributed very irregularly in space and time. It is very difficult to get quasi-continuous drifter observations at specific Eulerian locations. In addition, oscillations on periods close to tidal and inertial are usually very energetic in the velocity data. Inertial oscillations are usually caused by sharp variations of local wind during passages of atmospheric eddies or fronts. Their dynamics is described by the balance between terms (I) and (II) (and in some cases (IV)) of the equation (2), while term (III) is assumed to be small. In practice, inertial oscillations are not well-resolved by the satellite ARGO system determining drifter coordinates a few times every day (in some experiments, like WOCE, many drifter transmitters were on only

every third day). The kriging (one-dimentional optimal interpolation) used at NOAA/AOML to produce the 6-hourly dataset does not necessarily provide satisfactory description of the high-frequency velocity signal. Modern satellite altimeter supplies periodic data of the sea level anomaly at pretty amazing accuracy (few cm). However, satellite tracks are sparse in time and/or in space. Moreover, along-track data contain only one component of the vector (III) in (2). To make the altimetry data more friendly and practical, the Aviso (1996) fulfilled objective mapping of merged multi-satellite observations onto regular spatiotemporal grid. The price paid for this convenience is too large minimal temporal (10-15 days) and spatial (100-300 km) scales resolved.

Comparison between drifter and satellite altimetry data (Niiler et al., 2003a) shows that Aviso maps contain most of strong mesoscale eddies, but underestimate swirling velocities of the eddies. Niiler et al. (2003a) suggested to correct this difference by rescaling geostrophic velocity estimated from altimetry by regressing it linearly to the low-passed drifter velocities. Typically, the coefficient varied between 1.3 and 2 and the correction improved eddy statistics significantly. At the same time, large (185 cm) mean sea level difference across the Kuroshio Extension / Subarctic Front system, significantly exceeding expected value of 140-150 cm was recognized as an error of the method. Careful consideration did reveal the possibility of the bias occurring with the abovementioned correction. The problem with the correction procedure is that the same rescaling is applied to all spatial scales, while actual errors are on the smallest scale only. It is especially hard to suggest any reasonably simple improvement in the situation when velocity anomalies of different signs have different spatial scales. Figure 13 showing spatial distribution of the skewness of temporal variations of zonal component of geostrophic velocity proves that such a situation takes place in the reality. Multiple sources of the skewness include prevailing longitudinal variations of the velocity in the jets and preferred routs that eddies of different signs take in the ocean. However, it was estimated that errors due to such a bias are less than 10% and are not sufficient to explain the overestimations by Niiler et al. (2003a).

In the course of further study, more serious and more complex bias has been recognized. The source of this sort of the bias is in the mixed Eulerian-Lagrangian statitistical methods used. Namely, as high frequencies are missing in the mapped Aviso altimetry, Niiler et al. (2003a)

used the averaging in spatiotemporal bins to replace 6-hourly along-drifter-track data by the local monthly mean "independent observations" in regular spatial bins. As the faster drifter is moving the more bins it passes during the same time period, relative number of the resultant "independent observations" with larger velocities is larger than the relative number of the original 6-hourly fixes with the same large velocities. It was also shown that additional necessary conditions for this bias are low density of drifters and underestimated geostrophic velocities. Detailed description of the this study is provided by Maximenko (2003), who showed that all the mentioned conditions are satisfied and the bias gives rise to 30-50% overestimation of the mean velocities of all main jet currents and sea level differences across them.

References

Archiving, Validation, and Interpretation of Satellite Oceanographic Data (Aviso), in *Aviso Handbook for Merged TOPEX/Poseidon products*, 3rd ed., Toulouse, France, 1996.

Maximenko, N., Correspondence between Lagrangian and Eulerian velocity statistics at the ASUKA line, *J. Oceanogr.*, 2003 (in press). (Manuscript is available at http://iprc.soest.hawaii.edu/~nikolai/ASUKA_JO2003.pdf)

McWilliams, J. C., and J. M. Restrepo, The wave-driven ocean circulation, *J. Phys., Oceanog.*, **29**, 2523-2540, 1999.

Niiler, P.P., N.A. Maximenko, G.G. Panteleev, T. Yamagata, and D.B. Olson, Near-surface dynamical structure of the Kuroshio Extension. *J. Geophys. Res.-Oceans*, **108** (C6), 3193, 2003a.

Niiler, P. P., N. A. Maximenko, and J. C. McWilliams, Dynamically balanced absolute sea level of the global ocean derived from near-surface velocity observations, *Geophys. Res. Lett.*, **30** (22), 2164, doi:10.1029/2003GRL018628, 2003b.

Ralph, E. A., and P. P. Niiler, Wind driven currents in the tropical Pacific, *J. Phys., Oceanog.*, **29**, 2121-2129, 1999.

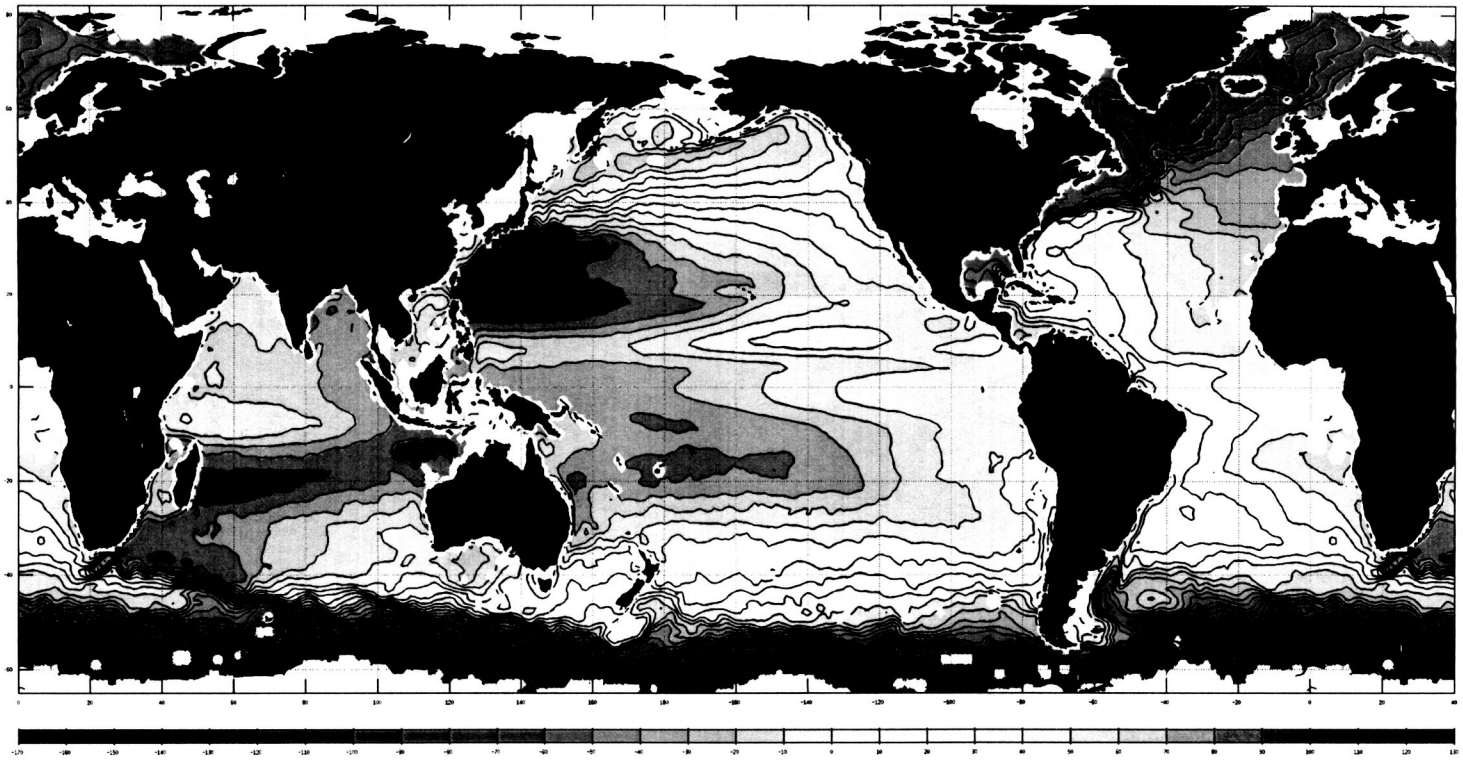

Figure 1. 1992-2002 absolute mean sea level (Niiler et al., 2003b). Contour interval is 10 cm.

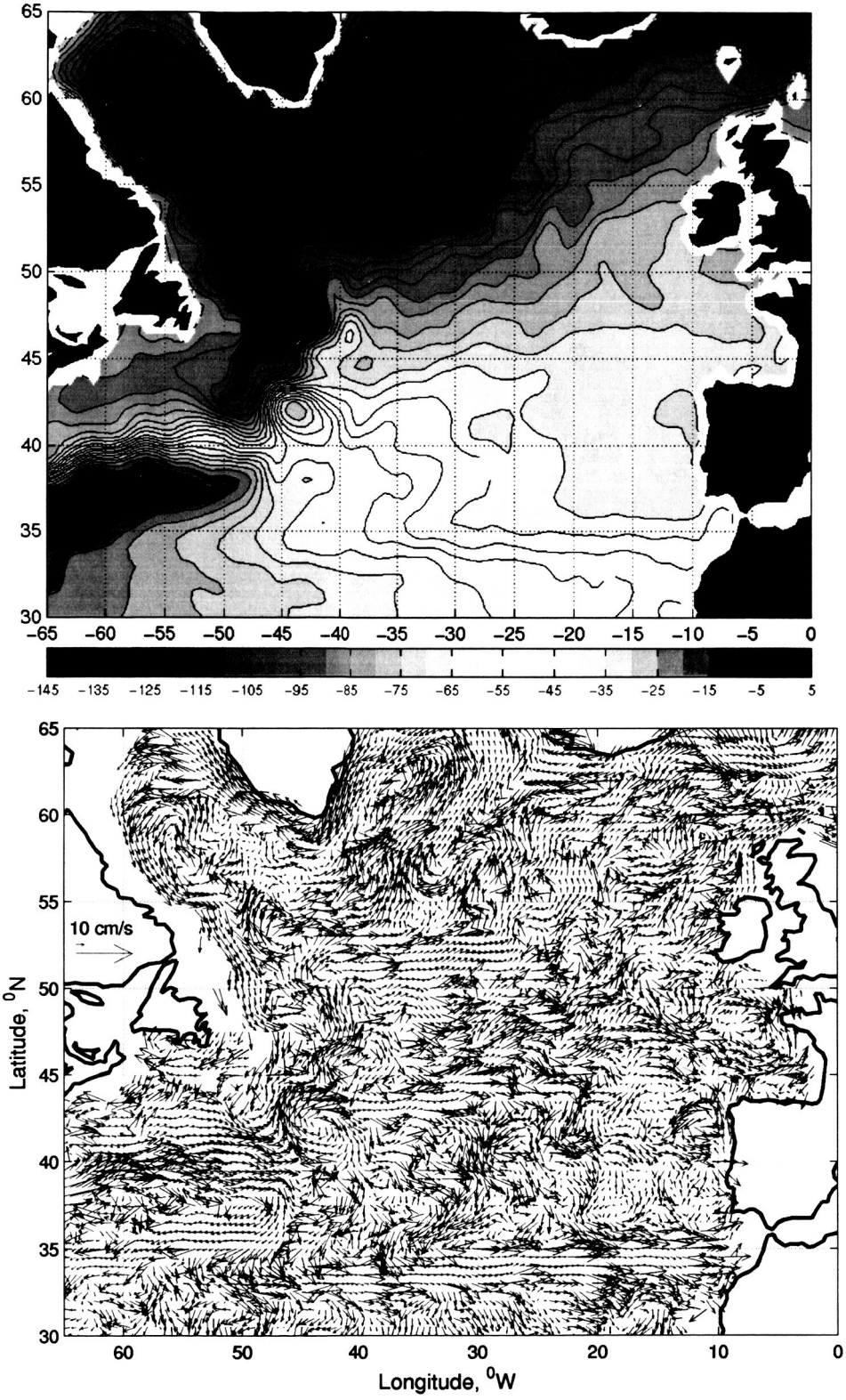

Figure 2. 1992-2002 mean sea level (upper) and geostrophic velocities in the North Atlantic. Contour interval is 5 cm. Velocities larger than 5 cm/s are shown in red and at different scale.

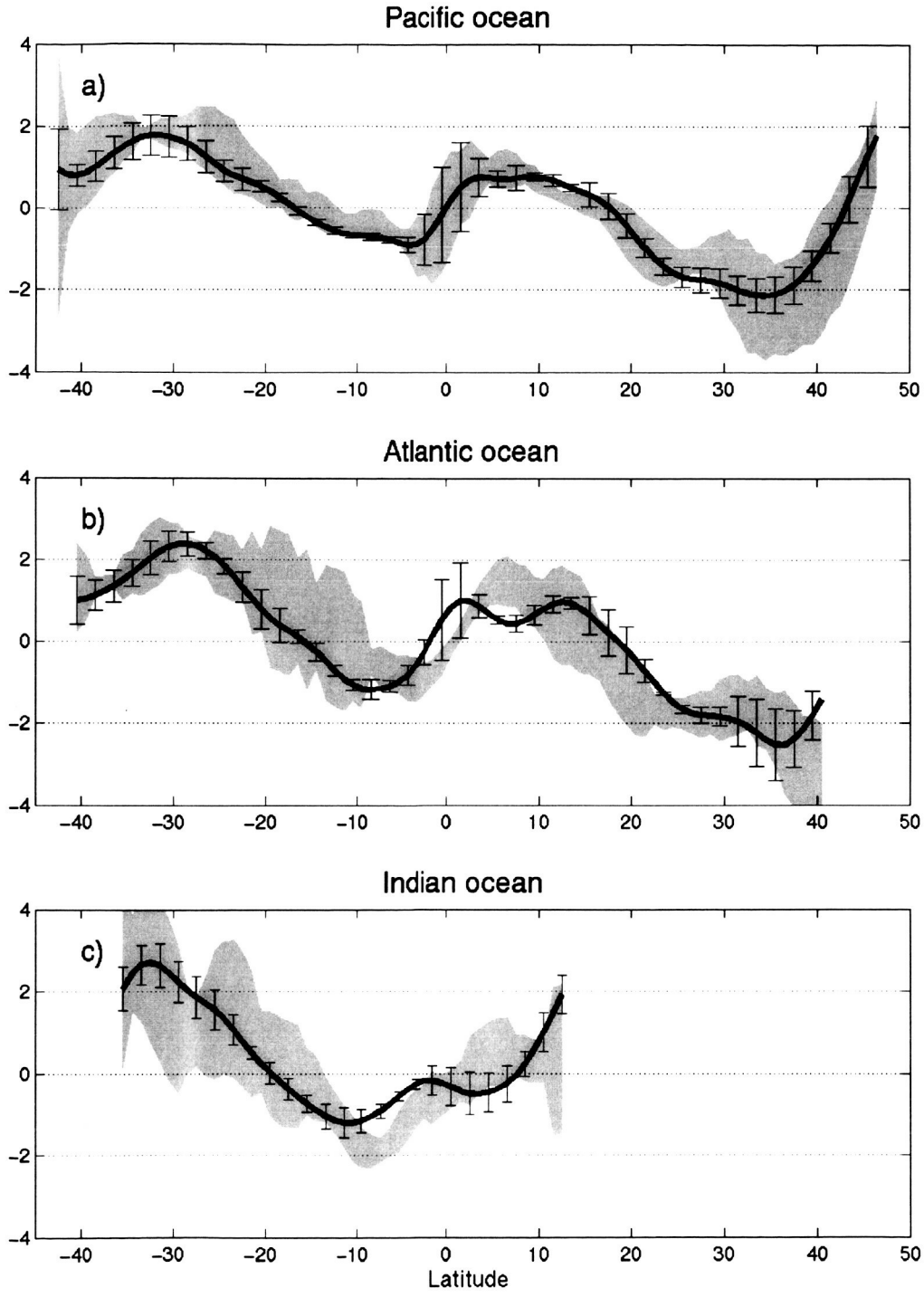

Figure 3. Zonal mean -curl($\partial\boldsymbol{\tau}$ / ∂z) /($\rho_0 g$) as expected from (1-2) (gray strips) and estimated from the NCAR/NCEP wind and Ralph and Niiler (1999) formula (3) in the Pacific (a), Atlantic (b) and Indian (c) oceans. Units are 10^{-15} s^{-1}.

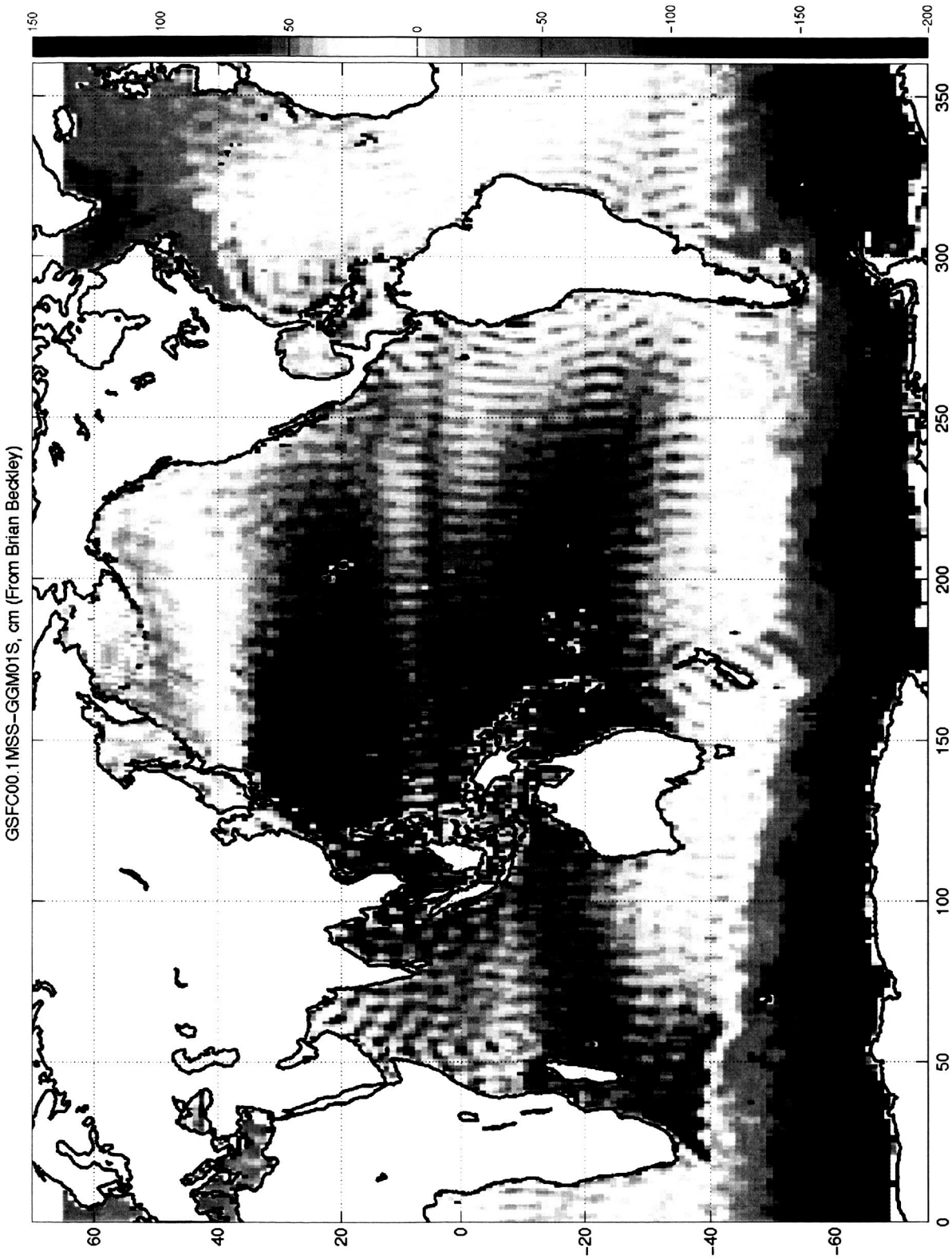

Figure 4. Mean sea level based on the first data of the GRACE mission computed at the NASA Goddard Space Flight Center to order and degree 90 (courtesy of Brian Beckley). Units are cm.

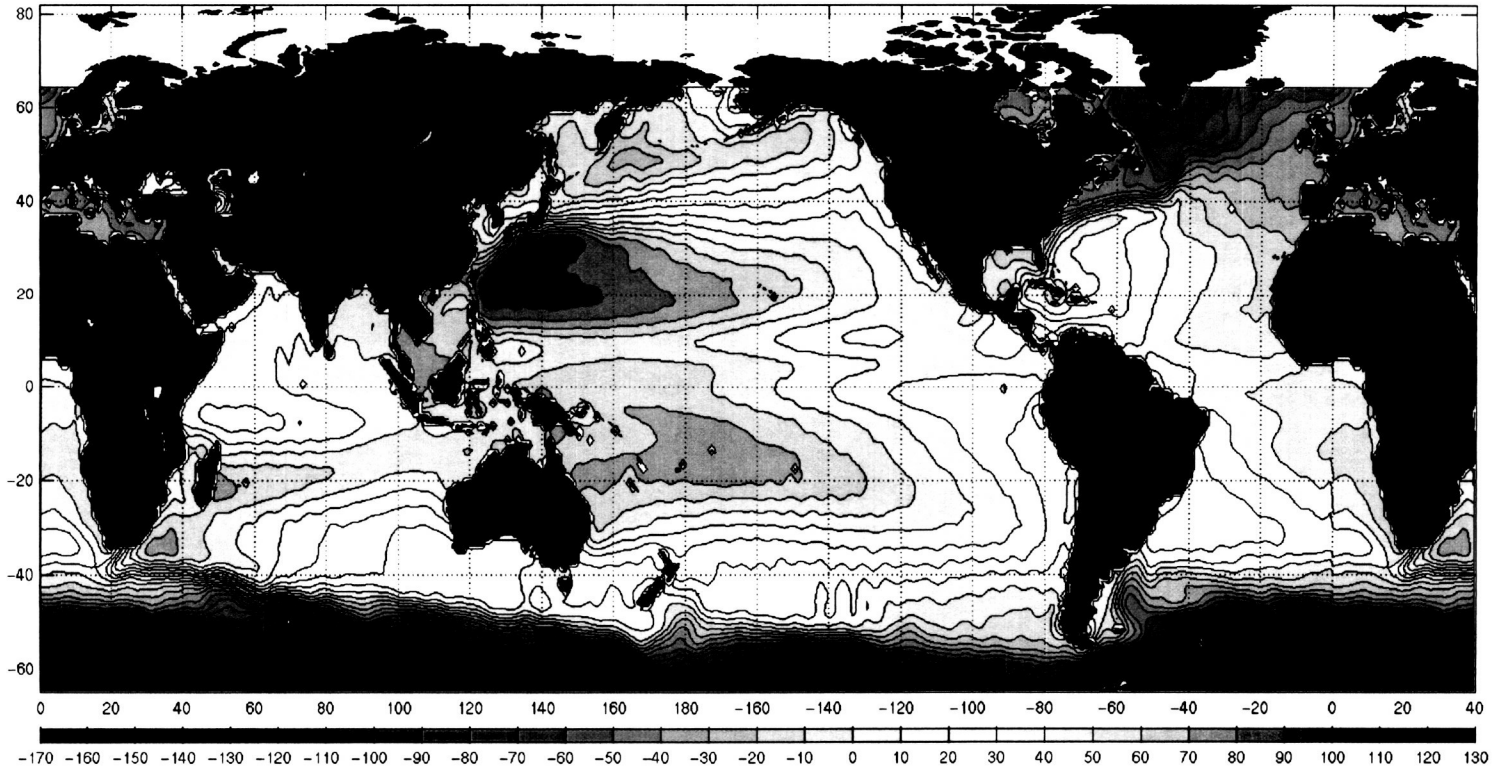

Figure 5. Smoothed mean sea level computed at the NASA Jet Propulsion Laboratory (courtesy of Victor Zlotnicky). Also similar to filter mean sea level shown in Figure 3. Contour interval is 10 cm.

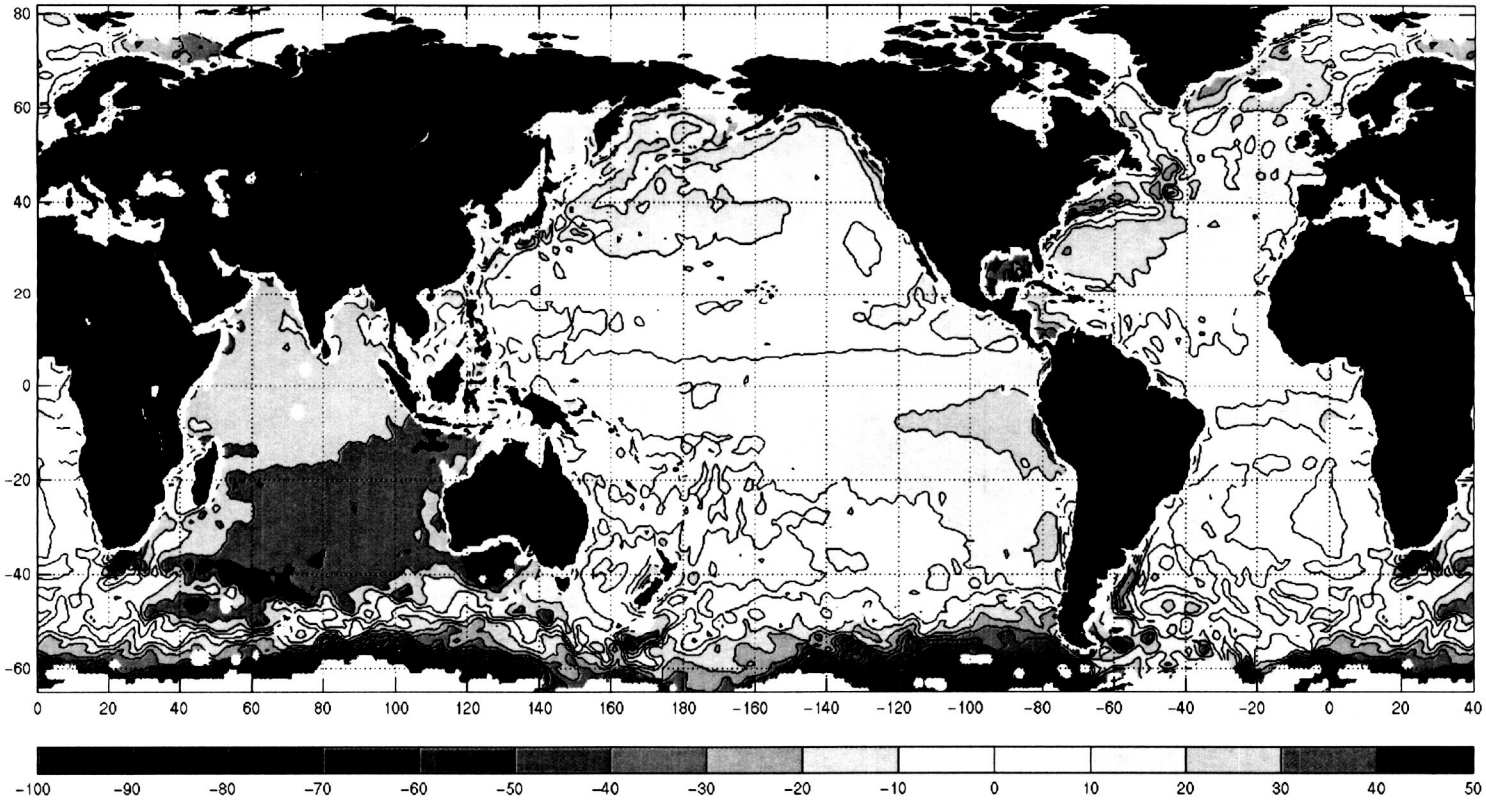

Figure 6. Difference between the sea levels shown in Figures 1 and 4. Contour interval is 10 cm.

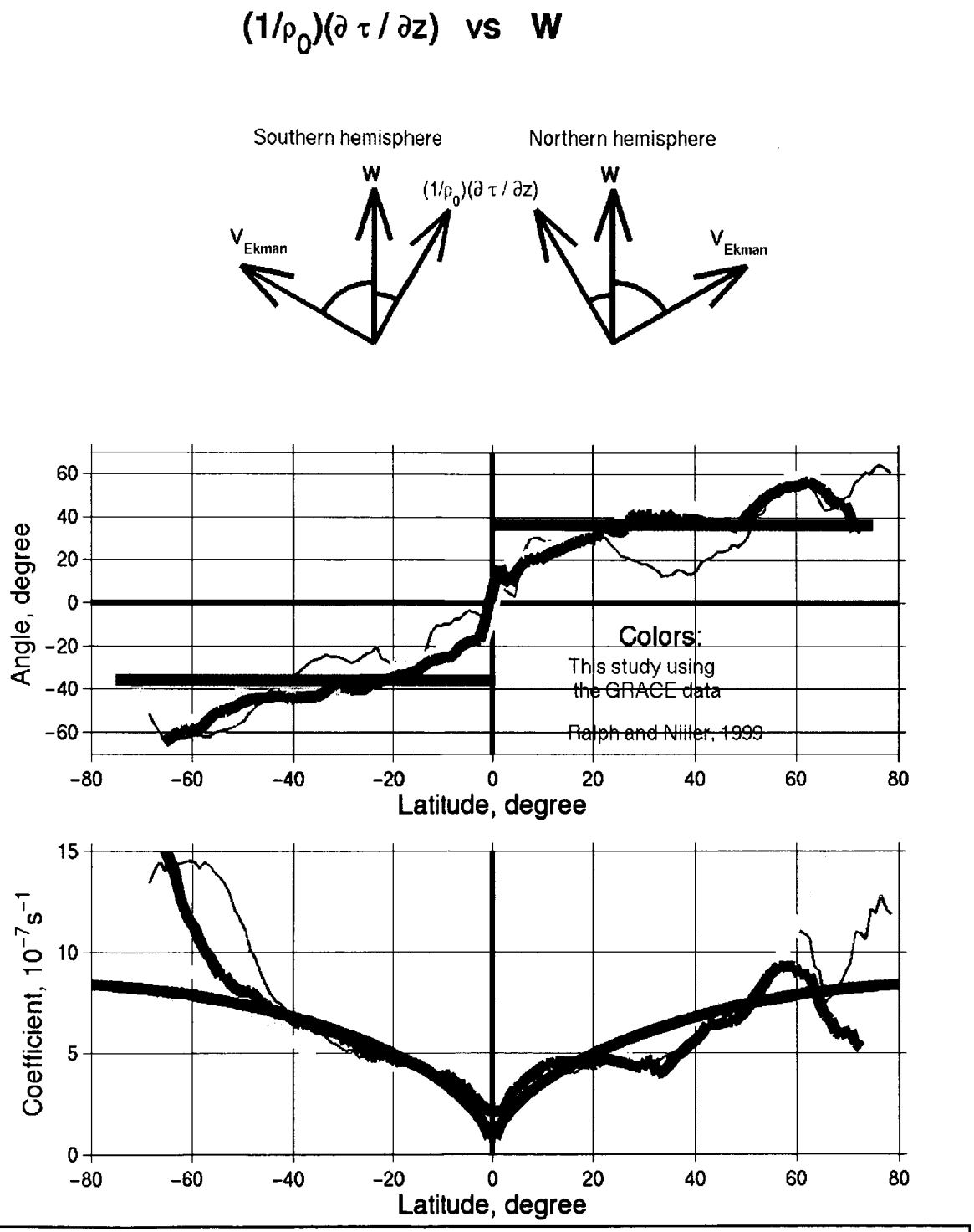

Figure 7. Optimal angle and coefficient between $\partial \boldsymbol{\tau} / \partial z / (\rho_0)$ and local NCAR/NCEP wind vector **W** as a function of latitude (dark blue). Red is for RN99 and green for drifters that lost their drogues.

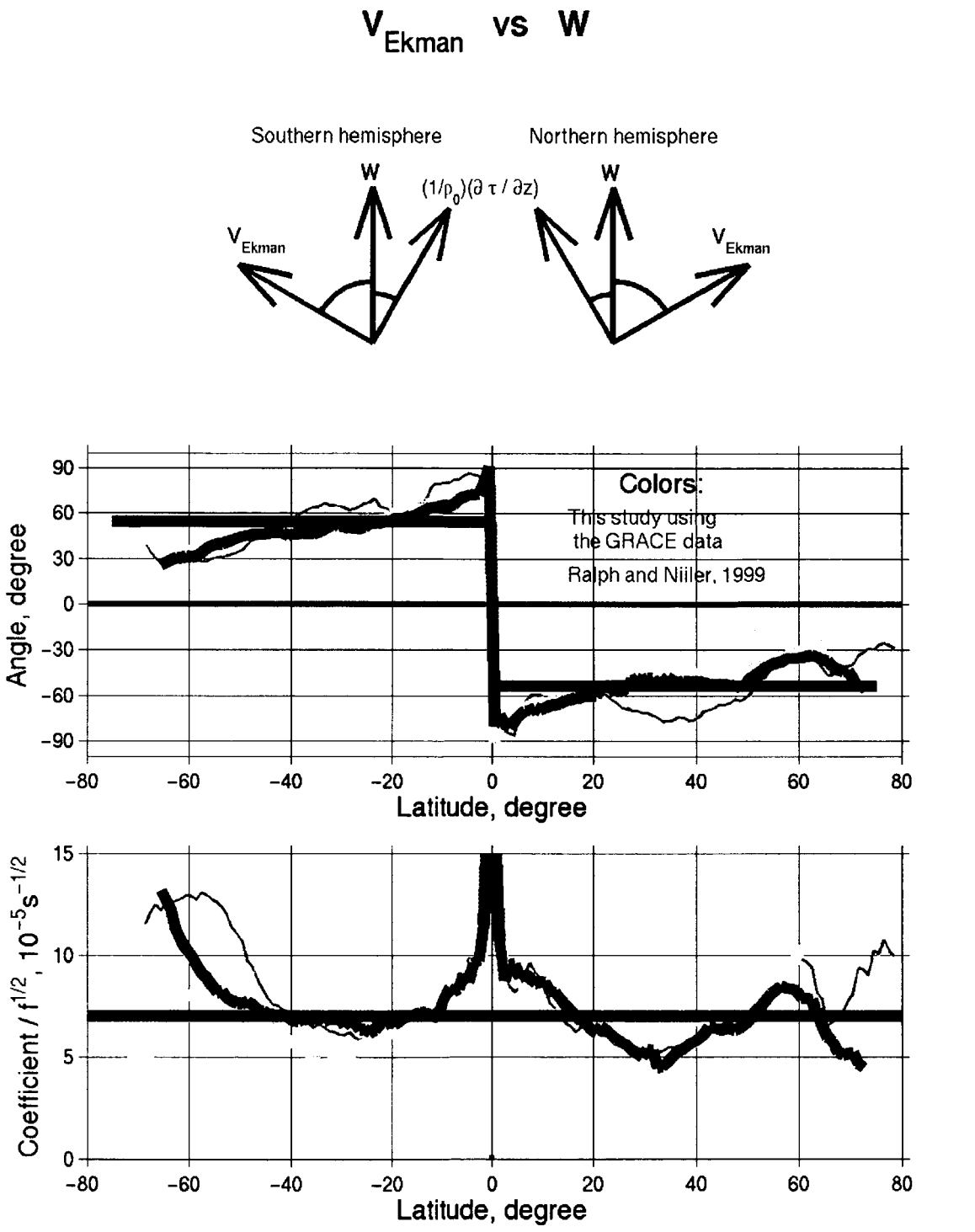

Figure 8. Same as Figure 7 but for the Ekman velocities.

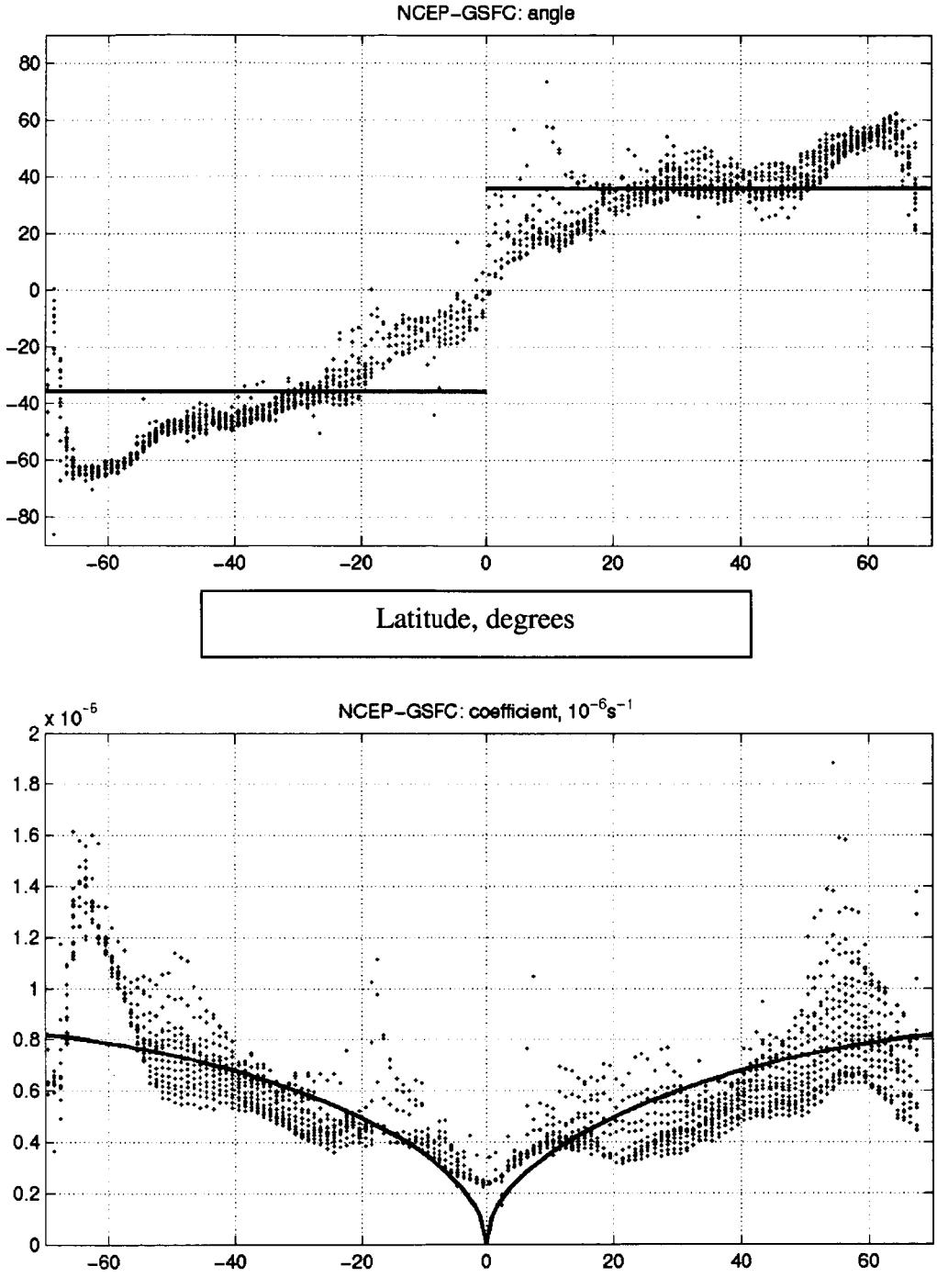

Figure 9. Optimal angle and coefficient between $\partial\tau / \partial z /(\rho_0)$ and local NCAR/NCEP wind vector **W**. Individual dots are for the 9^0 latitude x 3 m/s wind bins, centered on the 1^0 latitude x 1 m/s grid. Red are for the winds lower than 11 m/s. Black solid lines are RN99.

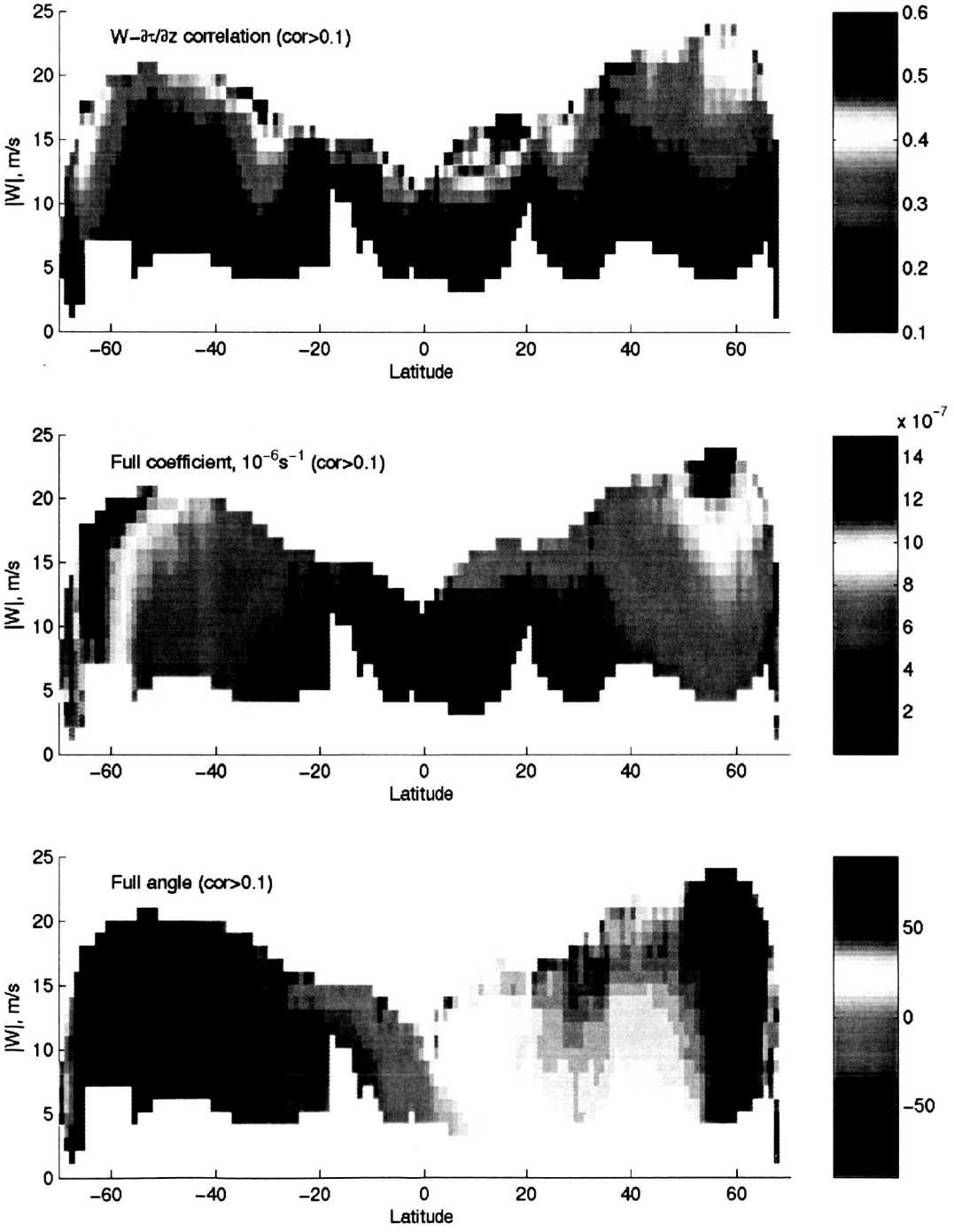

Figure 10. Correlation coefficient (CC) and optimal coefficient and angle between $\partial\boldsymbol{\tau} / \partial z /(\rho_0)$ and local NCAR/NCEP 10m wind vector **W**. Patches represent 9^0 latitude x 3 m/s wind bins, centered on 1^0 latitude x 1 m/s grid. Only bins with CC > 0.1 are shown.

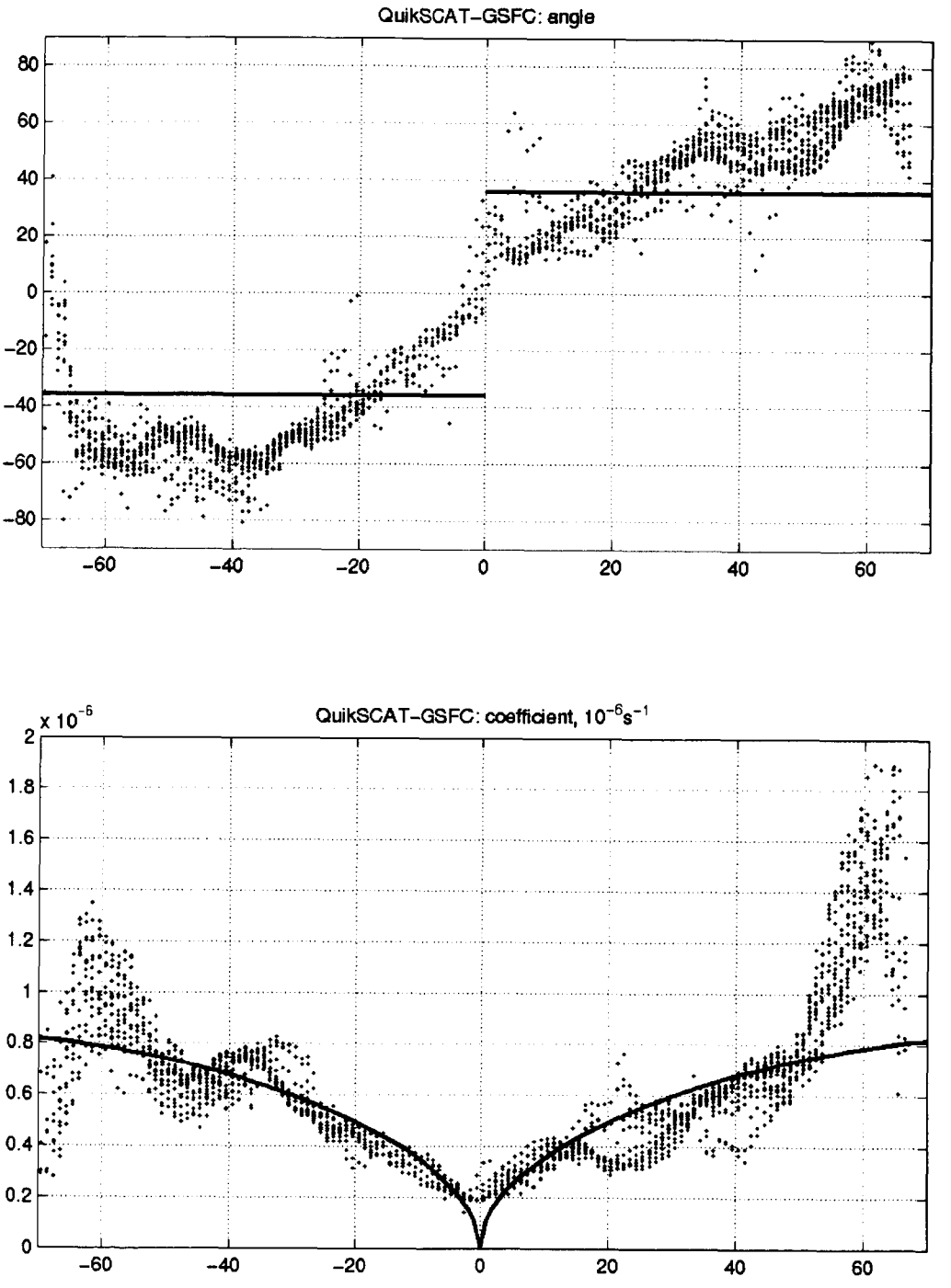

Figure 11. Same as Figure 9 but for the angle and coefficient between $\partial\boldsymbol{\tau} / \partial z /(\rho_0)$ and local QuikSCAT wind vector **W**.

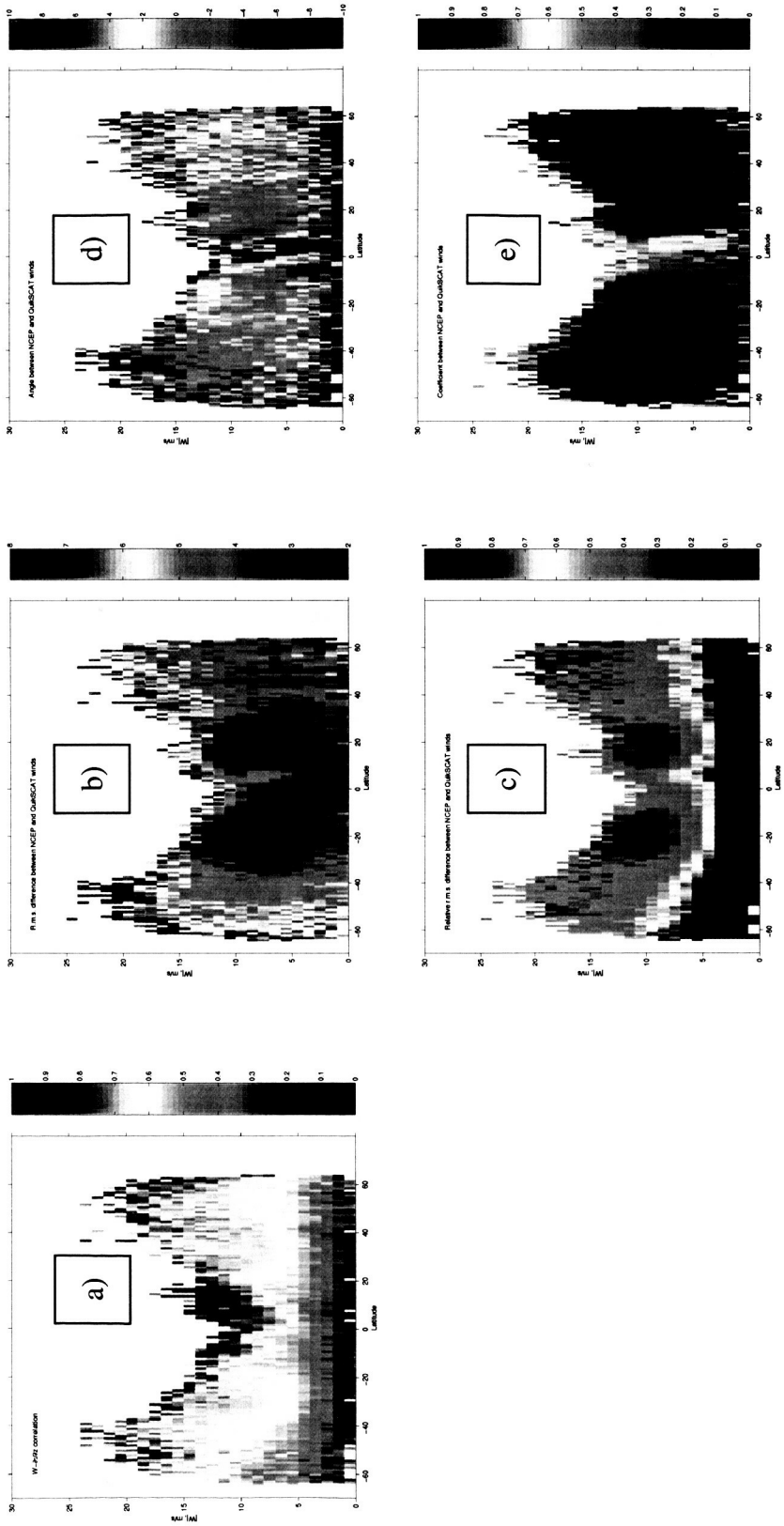

Fifure 12. Correlation coefficient (a), r.m.s. deviation (b), relative r.m.s.deviation (c), angle (d) and coefficient (e) between contemporaneous wind vectors at 10 m level from NCAR/NCEP and QuikSCAT datasets.

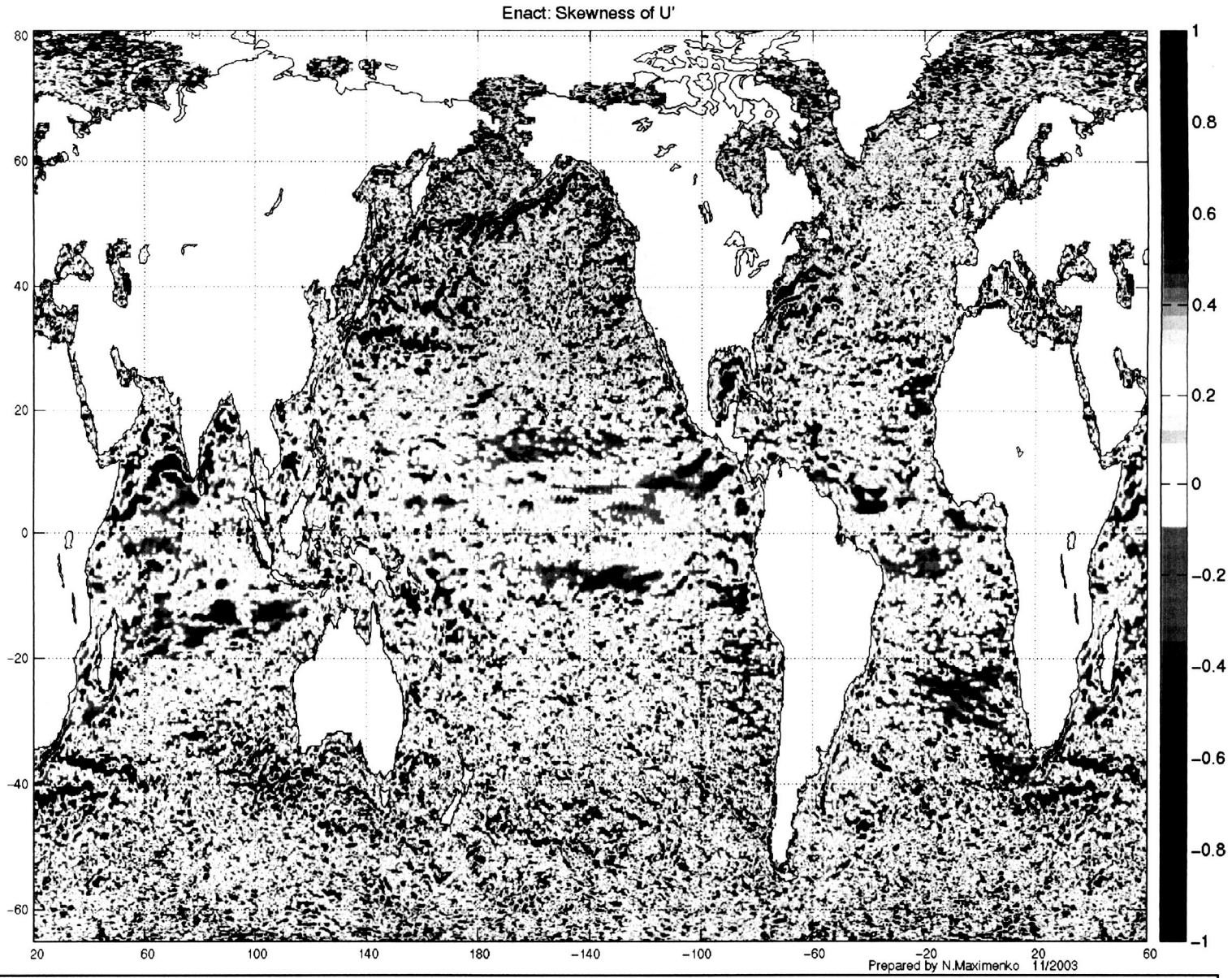

Figure 13. Skewness $\langle U'^3 \rangle / \langle U'^2 \rangle^{3/2}$ of temporal variations of zonal component of geostrophic velocity estimated from the Aviso maps.

PI contact information: Nikolai A. Maximenko
IPRC/SOEST, University of Hawaii,
1680 East West Road
Honolulu, HI 96822
Phone: (808) 956-2584
Fax: (808) 956-9425
E-mail: nikolai@soest.hawaii.edu